

Self-averaging in many-body quantum systems out of equilibrium: Time dependence of distributions

E. Jonathan Torres-Herrera,¹ Isaías Vallejo-Fabila,¹ Andrei J. Martínez-Mendoza,² and Lea F. Santos³

¹*Instituto de Física, Benemérita Universidad Autónoma de Puebla, Apt. Postal J-48, Puebla, 72570, Mexico*

²*División de Estudios de Posgrado e Investigación,*

Tecnológico Nacional de México/ Instituto Tecnológico de Oaxaca, C. P. 68030, Oaxaca de Juárez, Mexico

³*Department of Physics, Yeshiva University, New York City, New York, 10016, USA*

(Dated: May 29, 2020)

In a disordered system, a quantity is self-averaging when the ratio between its variance over disorder realizations and the square of its mean decreases as the system size increases. Here, we consider a chaotic disordered many-body quantum system out of equilibrium and identify which quantities are self-averaging and at which time scales. This is done by analyzing their distributions over disorder realizations. An exponential distribution, as found for the survival probability at long times, explains its lack of self-averaging, since the mean and the dispersion are equal. Gaussian distributions, on the other hand, are obtained for both self-averaging and non-self-averaging quantities. We also show that semi-analytical results for the self-averaging behavior of one quantity can be achieved from the knowledge of the distribution of another related quantity. This strategy circumvents numerical limitations on the sizes of the systems that we can deal with.

I. INTRODUCTION

Experimental advances with cold atoms [1], ion traps [2], superconducting devices [3], and nuclear magnetic resonance platforms [4, 5] allow for the high level of control and long coherence times of many-body quantum systems. This has invigorated experimental and theoretical studies of the long-time evolution of these systems. Common questions include the viability of thermalization [6–10], the description of the dynamics [11–13], and the time to reach equilibrium [14, 15]. Much less explored is the question of self-averaging [16–18].

One says that a quantity of a disordered system is self-averaging when its relative variance – the ratio between its variance over disorder realizations and the square of its mean – decreases as the system size increases. If self-averaging holds, as the system size increases, one can decrease the number of samples used in theoretical and experimental analyses. In this case, the properties of the system do not depend on the specific realization selected. In contrast, lack of self-averaging makes the study of disordered systems extremely challenging. Take as an example the scaling analysis of many-body quantum systems. The problem is already hard, because the many-body Hilbert space grows exponentially with system size. If in addition to this, one cannot decrease the number of disorder realizations for larger systems, the problem becomes intractable.

Non-self-averaging behavior is often associated with disordered many-body quantum systems at the metal-insulator transition [19] and systems at a critical point in general [20–27]. This sort of studies have mostly been done at equilibrium [21]. Recently, however, the analysis has been extended to systems out of equilibrium close to the metal-insulator transition [17, 18] and also in the chaotic regime [16]. An important conclusion is that self-averaging is not directly related with quantum

chaos [16, 28–30], as one might naively expect.

Quantum chaos refers to specific properties of the eigenvalues and eigenstates of systems that are chaotic in the classical limit. The eigenvalues are correlated [31–33] and the eigenstates are close to random vectors [9, 34], as in full random matrices. If the system shows these properties, it is usual to refer to it as chaotic even if one does not have its classical limit.

In Ref. [16], the analysis of self-averaging was done for both a disordered spin model in the chaotic regime and a model consisting of full random matrices of a Gaussian orthogonal ensemble (GOE). It was shown numerically and analytically that the survival probability (the probability for finding the system in its initial state at a later time) is non-self-averaging at any time scale. Other quantities considered include the inverse participation ratio, which measures the spread of the initial state in the many-body Hilbert space, and observables measured in experiments with cold atoms and ion traps, namely the spin autocorrelation function and the connected spin-spin correlation function. The self-averaging behavior of these quantities varies in time.

Motivated by those results, we now study numerically and analytically the distributions over disorder realizations of those same quantities. In addition, we consider also of the absolute value and the square of the spin autocorrelation function. Our goal is to understand how the shape and overall properties of the distributions depend on time, observables, and models, and whether they can help us determine when self-averaging holds.

We find that at short times, the distributions are model dependent. Due to the locality of the spin model Hamiltonian, the distributions of the quantities considered here exhibit a fragmented structure with peaks at different energy windows, while they are Gaussian for the GOE model.

At long times, the distributions become similar for both models, but they differ depending on the quantity.

The survival probability, for example, shows an exponential distribution [28–30, 35] as soon as the correlations between the eigenvalues get manifested in the dynamics. This distribution, where mean and standard deviation coincide, explains the lack of self-averaging of this quantity at long times.

By comparing the shape of the distributions with the presence of self-averaging, we conclude that the two are not correlated. In particular, Gaussian distributions are found for both self-averaging and non-self-averaging quantities.

We show, however, that knowledge of the shape of the distribution for one quantity can assist us to determine the self-averaging behavior of another related quantity. As an example, we discuss the case of the spin autocorrelation function, $I(t)$, and its absolute value, $|I(t)|$. The numerical analysis of the self-averaging behavior of $|I(t)|$ at long times are inconclusive, due to the limitation to small system sizes. However, in hands of the Gaussian distribution for $I(t)$, we find analytically the dependence on system size of the relative variance of $|I(t)|$. With this strategy, we are able to deduce that $|I(t)|$ is non-self-averaging at long times.

The paper is organized as follows. After presenting the model, initial states, and quantities in Sec. II and discussing the dynamics and self-averaging properties of the observables in Sec. III, we proceed with the analysis of the distributions in Secs. IV, V, and VI. This study is separated by time intervals: short times in Sec. IV, long times in Sec. V, and intermediate times in Sec. VI. Conclusions are presented in Sec. VII.

II. MODELS, INITIAL STATES, AND QUANTITIES

We study two models described by Hamiltonians of the form

$$H = H_0 + V, \quad (1)$$

where H_0 is the unperturbed part of the total Hamiltonian and V is a strong perturbation that takes the system into the chaotic regime. The notation adopted is the following: $|n\rangle$ stands for the eigenstates of H_0 , $|\alpha\rangle$ for the eigenstates of H , and E_α for the eigenvalues of H . One model consists of random matrices from a GOE and the other is a many-body spin-1/2 system.

A. GOE model

For the GOE model, H_0 is the diagonal part of a full random matrix of dimension D and V contains the off-diagonal elements. The entries are all real random numbers from a Gaussian distribution with mean value $\langle H_{ij} \rangle = 0$ and variance

$$\langle H_{ij}^2 \rangle = \begin{cases} 1 & i = j \\ 1/2 & i \neq j \end{cases} \quad (2)$$

The Hamiltonian matrix H can be generated by creating a matrix M with random numbers from a Gaussian distribution with mean 0 and variance 1 and then adding M to its transpose as $H = (M + M^T)/2$ [36]. The eigenvalues of this model are highly correlated [31–33] and the eigenstates are normalized random vectors [34]. There are no realistic systems described by this model, but it allows for analytical derivations not only for static properties [31, 33, 37], but also for the dynamics [14, 16, 38].

B. Disordered spin model

We consider a one-dimensional chaotic spin-1/2 model of experimental interest [39] and used in studies of many-body localization [40–45]. It has onsite disorder and nearest neighboring couplings [46, 47],

$$\begin{aligned} H_0 &= J \sum_{k=1}^L (h_k S_k^z + S_k^z S_{k+1}^z), \\ V &= J \sum_{k=1}^L (S_k^x S_{k+1}^x + S_k^y S_{k+1}^y). \end{aligned} \quad (3)$$

Above, $\hbar = 1$, $S_k^{x,y,z}$ are spin operators on site k , L is the size of the chain, which is even throughout this work, periodic boundary conditions are used, and $J = 1$ is the coupling strength. The Zeeman splittings h_i are random numbers uniformly distributed in $[-h, h]$. The total magnetization in the z -direction is conserved and we take the largest subspace, where the total z -magnetization is zero and the dimension is $D = L!/(L/2)!^2$. We use disorder strength $h = 0.75$, which places the system in the chaotic regime. The level statistics and the structure of the eigenstates away from the borders of the spectrum are comparable to those of the GOE model.

C. Initial state

The initial state $|\text{ini}\rangle = |\Psi(0)\rangle$ is an eigenstate $|n\rangle = |\text{ini}\rangle$ of H_0 . We take $|\Psi(0)\rangle$ with energy close to the middle of the spectrum, where the eigenstates are chaotic [9, 48],

$$E_{\text{ini}} = \langle \Psi(0) | H | \Psi(0) \rangle = \sum_{\alpha} |C_{\alpha}^{\text{ini}}|^2 E_{\alpha} \sim 0, \quad (4)$$

with

$$C_{\alpha}^{\text{ini}} = \langle \alpha | \Psi(0) \rangle. \quad (5)$$

For the spin model, the initial states are product states in the z -direction, where on each site the spin either points up or down in the z -direction, such as $|\uparrow\downarrow\uparrow\downarrow\uparrow\dots\rangle$. They are often referred to as site-basis vectors or computational basis vectors.

D. Quantities

We analyze in detail the distributions over disorder realization of the survival probability and the inverse participation ratio. Both are non-local in space. We also present results for the spin autocorrelation function, its absolute value and its square, and the connected spin-spin correlation function. These four quantities are local in space.

Our studies of the survival probability and the inverse participation ratio are presented for the GOE model and the chaotic spin model. For the local quantities, this is done only for the spin model, since the notion of locality does not exist in full random matrices.

The survival probability is the squared overlap of the initial state and its evolved counterpart,

$$P_S(t) = |\langle \Psi(0) | e^{-iHt} | \Psi(0) \rangle|^2 = \left| \sum_{\alpha} |C_{\alpha}^{\text{ini}}|^2 e^{-iE_{\alpha}t} \right|^2 = \left| \int dE e^{-iEt} \rho_{\text{ini}}(E) \right|^2, \quad (6)$$

where

$$\rho_{\text{ini}}(E) = \sum_{\alpha} |C_{\alpha}^{\text{ini}}|^2 \delta(E - E_{\alpha}) \quad (7)$$

is the energy distribution of the initial state. $\rho_{\text{ini}}(E)$ is usually referred to as local density of states (LDOS) or strength function. The width Γ of this distribution depends on the number of states $|n\rangle$ that are directly coupled with $|\Psi(0)\rangle$,

$$\begin{aligned} \Gamma^2 &= \sum_{\alpha} |C_{\alpha}^{\text{ini}}|^2 E_{\alpha}^2 - \left(\sum_{\alpha} |C_{\alpha}^{\text{ini}}|^2 E_{\alpha} \right)^2 \\ &= \langle \Psi(0) | HH | \Psi(0) \rangle - \langle \Psi(0) | H | \Psi(0) \rangle^2 \\ &= \sum_n \langle \Psi(0) | H | n \rangle \langle n | H | \Psi(0) \rangle - \langle \Psi(0) | H | \Psi(0) \rangle^2 \\ &= \sum_{n \neq \text{ini}} |\langle n | H | \Psi(0) \rangle|^2. \end{aligned} \quad (8)$$

The survival probability is a quantity of great theoretical and experimental [49] relevance. It has been used in studies of the quantum speed limit [50, 51], onset of exponential [52, 53] and power-law [54–58] decays, quench dynamics [59–64], ground state and excited state quantum phase transitions [65, 66], quantum scars [67, 68], multifractality in disordered systems [69–72], and emergence of the correlation hole [73–78].

The inverse participation ratio measures the spreading of the initial many-body state in the basis of unperturbed many-body states $|n\rangle$ [79, 80]. It is defined as

$$\text{IPR}(t) = \sum_n |\langle n | e^{-iHt} | \Psi(0) \rangle|^4. \quad (9)$$

At $t = 0$, when $|\Psi(0)\rangle$ is one of the states $|n\rangle$, $\text{IPR}(t) = 1$. As $|\Psi(0)\rangle$ spreads into other states $|n\rangle$, $\text{IPR}(t)$ decays.

For chaotic systems perturbed far from equilibrium, it reaches very small values.

The spin autocorrelation function measures the proximity of a spin k at time t to its orientation at $t = 0$ and it is averaged over all sites,

$$I(t) = \frac{4}{L} \sum_{k=1}^L \langle \Psi(0) | S_k^z e^{iHt} S_k^z e^{-iHt} | \Psi(0) \rangle. \quad (10)$$

This quantity is equivalent to the density imbalance between even and odd sites measured in experiments with cold atoms [39], as can be seen by mapping the spins into hardcore bosons. The self-averaging behavior of this quantity was studied in [16, 17]. Here, we analyze also $|I(t)|$ and $I^2(t)$. This is done because at long times, $I(t)$ can reach negative values and the oscillations between negative and positive values may complicate the analysis of self-averaging, which is avoided with the other two quantities.

The connected spin-spin correlation function is given by

$$C(t) = \frac{4}{L} \sum_k [\langle \Psi(t) | S_k^z S_{k+1}^z | \Psi(t) \rangle - \langle \Psi(t) | S_k^z | \Psi(t) \rangle \langle \Psi(t) | S_{k+1}^z | \Psi(t) \rangle] \quad (11)$$

and is measured in experiments with ion traps [81].

III. DYNAMICS AND SELF-AVERAGING

This section describes the evolution of the mean and of the relative variance of the six quantities considered in this work. Part of these results were already discussed in Refs. [14, 16], but they are needed to explain the distributions presented in the next sections.

A quantity O is self-averaging when its relative variance

$$\mathcal{R}_O(t) = \frac{\sigma_O^2(t)}{\langle O(t) \rangle^2} = \frac{\langle O^2(t) \rangle - \langle O(t) \rangle^2}{\langle O(t) \rangle^2} \quad (12)$$

decreases as the system size increases. The notation $\langle \cdot \rangle$ indicates here the average over disorder realizations and initial states. We consider $0.01D$ initial states and at least $10^4/(0.01D)$ disorder realizations, so that each point for the curves of $\langle O(t) \rangle$ and $\mathcal{R}_O(t)$ is an average over 10^4 data.

A. Survival Probability

In the top panels of Fig. 1, we show the LDOS $\rho_{\text{ini}}(E)$ for the GOE model, which is a semicircle [Fig. 1 (a)], and for the spin model, which is Gaussian [Fig. 1 (b)]. The shape and bounds of the LDOS determine the initial decay of the survival probability. Following Eq. (6), the square of the Fourier transform of a semicircle gives

$\mathcal{J}_1^2(2\Gamma t)/(\Gamma^2 t^2)$, where \mathcal{J}_1 indicates the Bessel function of the first kind [59, 60]. This implies that after a very rapid initial decay, $\langle P_S(t) \rangle$ shows oscillations that decay according to a power law $\propto t^{-3}$ [57, 58], as seen in Fig. 1 (c). The square of the Fourier transform of a bounded Gaussian gives $\exp(-\Gamma^2 t^2)\mathcal{F}(t)/(4\mathcal{N}^2)$, where $\mathcal{F}(t)$ involves error functions and \mathcal{N} is a normalization constant (see the appendices in Refs. [14, 58]). This implies that after an initial Gaussian decay [59, 60], $\langle P_S(t) \rangle$ shows a power-law behavior $\propto t^2$ [57, 58, 82], as observed in Fig. 1 (d).

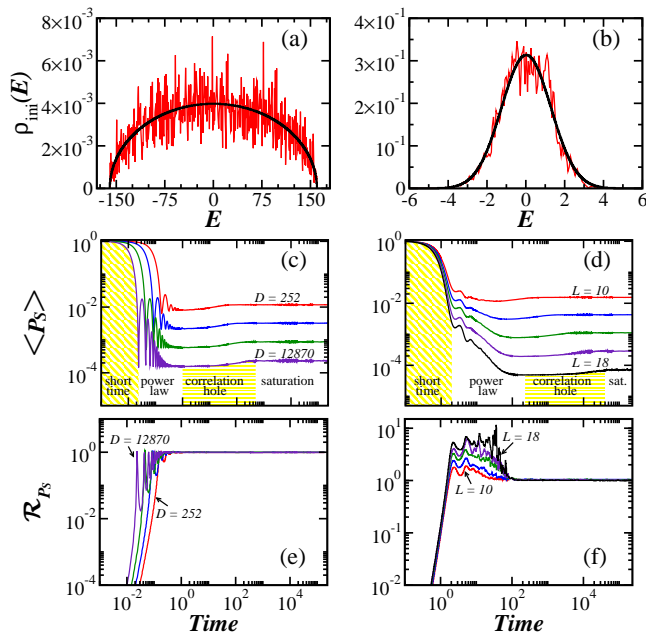


FIG. 1. Local density of states [(a) and (b)], evolution of the mean of the survival probability [(c) and (d)], and evolution of the relative variance of the survival probability [(e) and (f)] for the GOE model (left panels) and the chaotic disordered spin model (right panels). The time intervals for the fast initial decay, power-law behavior, correlation hole, and saturation are indicated in Fig. 1 (c) and (d). In Fig. 1 (a) and (b): $D = 12870$, which implies $L = 16$ for the spin model. In Fig. 1 (c)-(f): $D = 252, 924, 3432, 12870$ ($L = 10, 12, 14, 16$). For the spin model, $L = 18$ is also shown. In Fig. 1 (a) and (b): one initial state and one disorder realization; in Fig. 1 (c)-(f): $0.01D$ disorder realizations and $10^4/(0.01D)$ initial states.

The power-law decays in Fig. 1 (c) and Fig. 1 (d) persist up to a time denoted by t_{Th} [14], where $\langle P_S(t) \rangle$ reaches its minimum value. Beyond this point, the survival probability increases until the dynamics saturates for $t > t_{\text{R}}$, where t_{R} is the relaxation time. At this point, $\langle P_S(t > t_{\text{R}}) \rangle$ fluctuates around the infinite-time average $\langle \sum_{\alpha} |C_{\alpha}^{\text{ini}}|^4 \rangle$. The dip below the saturation point is known as correlation hole [73–75] and it appears only in systems where the eigenvalues are correlated.

The four time intervals for the distinct behaviors of $\langle P_S(t) \rangle$ – fast initial decay, power-law behavior, correlation hole, and saturation – are indicated in Fig. 1 (c) and

Fig. 1 (d). These are the time scales that we consider in the next sections to investigate the distributions of the survival probability and the other quantities as well.

In Fig. 1 (e) and Fig. 1 (f), we show results for the relative variance $\mathcal{R}_{P_S}(t)$ for different system sizes. The survival probability is non-self-averaging at any time scale, as shown analytically in Ref. [16]. Initially, $\mathcal{R}_{P_S}(t)$ grows with system size, while for $t > t_{\text{Th}}$, it reaches a constant value, $\mathcal{R}_{P_S}(t) \sim 1$. There is no noticeable difference in the value of $\mathcal{R}_{P_S}(t)$ in the interval $[t_{\text{Th}}, t_{\text{R}}]$ and for $t > t_{\text{R}}$.

B. Inverse Participation Ratio

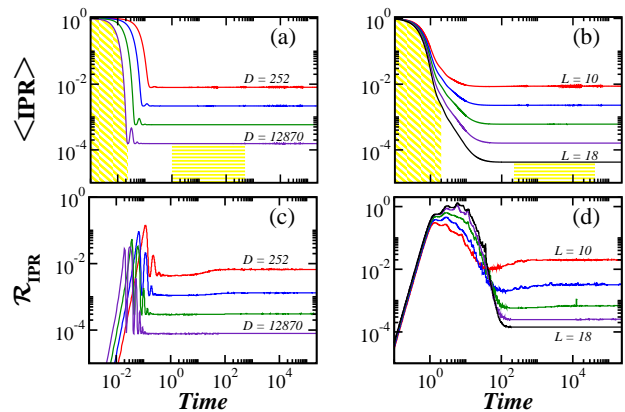


FIG. 2. Evolution of the mean of the inverse participation ratio [(a) and (b)], and evolution of the relative variance of the inverse participation ratio [(c) and (d)] for the GOE model (left panels) and the chaotic disordered spin model (right panels). The four time intervals identified in the evolution of the survival probability are indicated here as well. The system sizes are $D = 252, 924, 3432, 12870$ ($L = 10, 12, 14, 16$); for the spin model, $L = 18$ is also used. In all panels: $0.01D$ disorder realizations and $10^4/(0.01D)$ initial states.

Figure 2 shows the dynamics and self-averaging behavior of the inverse participation ratio for the same time scales as in Fig. 1. As seen in Fig. 2 (a) and Fig. 2 (b), there are two different behaviors for $\langle \text{IPR}(t) \rangle$ at short times. The decay is initially very fast and then it either oscillates in the case of the GOE model [Fig. 2 (a)] or it slows down for the spin model [Fig. 2 (b)]. These two time scales coincide with the intervals for the fast decay and the power-law behavior of $\langle P_S(t) \rangle$. Beyond this point, however, a correlation hole is not visible for $\langle \text{IPR}(t) \rangle$. It exists, but it is extremely small [14] and, contrary to what we find for the survival probability, the ratio between the saturation point of $\langle \text{IPR}(t) \rangle$ and its minimum value at the correlation hole decreases as the system size increases.

The evolution of the relative variance can be seen in Fig. 2 (c) and Fig. 2 (d). It shows that the inverse participation ratio is non-self-averaging at short times, which is understandable, since for small times, $\langle \text{IPR}(t) \rangle \sim \langle P_S^2(t) \rangle$. But for times $t > t_{\text{Th}}$, the inverse participation ratio

becomes “super” self-averaging, by which we mean that $\mathcal{R}_{\text{IPR}}(t) \propto 1/D$ instead of $\propto 1/L$.

C. Local Quantities

The local quantities are self-averaging up to the correlation hole. The connected spin-spin correlation function does not detect the hole and remains self-averaging at all times [16]. In contrast, the spin autocorrelation function exhibits a correlation hole and stops being self-averaging beyond its minimum value.

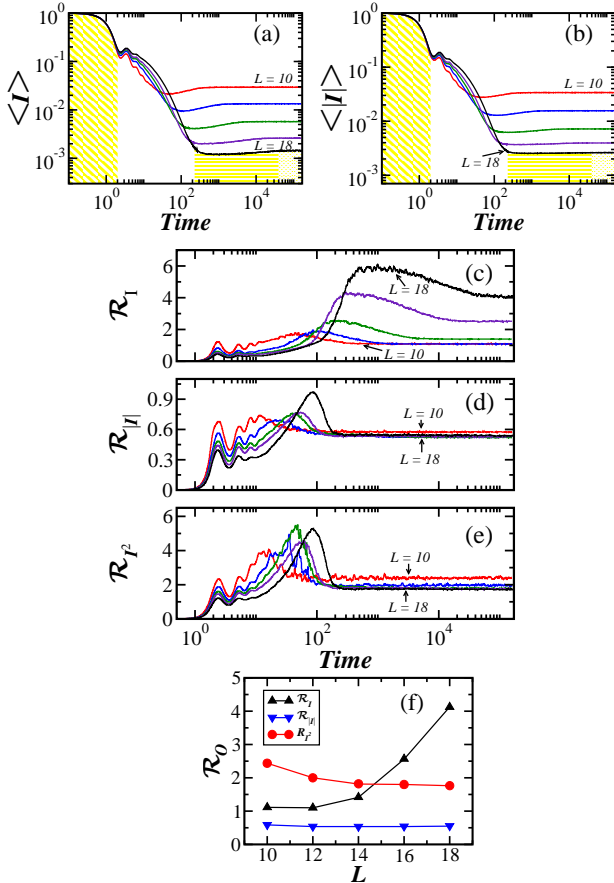


FIG. 3. Evolution of the mean of the spin autocorrelation function (a) and its relative variance (c), the mean of the absolute value of the spin autocorrelation function (b) and its relative variance (d), the relative variance of the squared imbalance (e), and the relative variance for $t > t_R$ vs L (f) for the chaotic disordered spin model. In (a), (b): The four time intervals identified in the evolution of the survival probability are indicated and the system sizes are $L = 10, 12, 14, 16, 18$. The average is over 10^4 data and (f) also includes an average for 100 different instants of times.

In Fig. 3 (a) and (b), we show the results for the mean of the spin autocorrelation function and for the mean of its absolute value. The correlation hole is less evident for $\langle |I(t)| \rangle$ and for $\langle I^2(t) \rangle$ (this one is not shown) than for $\langle I(t) \rangle$, but it is still present. For the three quanti-

ties, however, the ratio between the saturation point and the minimum of the hole decreases as L increases, which contrasts with the survival probability, where the ratio is constant.

The three quantities are self-averaging at short times, with $\mathcal{R}_{I,|I|,I^2}(t)$ decreasing as L increases [see Fig. 3 (c), (d) and (e)]. For $t \sim t_{\text{Th}}$, the curves cross. Beyond this point, for $t > t_{\text{Th}}$, the behavior of $\mathcal{R}_I(t)$, $\mathcal{R}_{|I|}(t)$, and $\mathcal{R}_{I^2}(t)$ differ. $\mathcal{R}_I(t)$ increases with system size, indicating non-self-averaging, while the curves for $\mathcal{R}_{I^2}(t)$ cross once again, recovering self-averaging at long times. $\mathcal{R}_{|I|}(t)$, on the other hand, is nearly constant, suggesting lack of self-averaging, but it is not possible to make a conclusive statement based on the few system sizes available. The scalings of $\mathcal{R}_I(t)$, $\mathcal{R}_{|I|}(t)$, and $\mathcal{R}_{I^2}(t)$ with L are chosen in Fig. 3 (f).

As discussed in Sec. V C, the analysis of the distribution of $I(t)$ helps us determine whether $\mathcal{R}_{|I|}(t > t_R)$ is indeed independent of L . The strategy of using one quantity in the self-averaging study of another one is an important result of this work.

We decided to study $|I(t)|$ and $I^2(t)$, in addition to $I(t)$, because the latter occasionally reaches negative values at long times, which could suggest that $\mathcal{R}_I(t)$ increases with L just because $\langle I(t) \rangle$ gets very close to zero. We stress, however, that $\langle I(t) \rangle$ saturates at values larger than the saturation values of $\langle \text{IPR}(t) \rangle$ and $\langle I^2(t) \rangle$, and yet, these two quantities are self-averaging at long times. The point is not whether $\langle O(t) \rangle^2$ decreases with L , but whether it decreases slower than $\sigma_O^2(t)$. The mean is the reference with respect to which the dispersion can be said to be large or small.

IV. DISTRIBUTIONS AT SHORT TIMES

In Fig. 4, we show the distributions of the survival probability [(a) and (b)] and the inverse participation ratio [(c) and (d)] for the GOE model [(a) and (c)] and the spin model [(b) and (d)] at very short times, $t < \Gamma^{-1}$, when the decays of $\langle P_S(t) \rangle$ and $\langle \text{IPR}(t) \rangle$ are very fast. The distributions are similar for both quantities, but differ between the models.

In this section, we discuss also the distributions for the local quantities, which are studied only for the spin model. They are similar to those for $\langle P_S(t) \rangle$ and $\langle \text{IPR}(t) \rangle$ in Figs. 4 (b) and (d).

A. Survival Probability

At short times, the decay of the survival probability is controlled by the short-time expansion of $\mathcal{J}_1^2(2\Gamma t)/(\Gamma^2 t^2)$ for the GOE model and of $\exp(-\Gamma^2 t^2)$ for the spin model. The distribution of $P_S(t)$ at a fixed time $t < \Gamma^{-1}$ reflects then the distribution of Γ^2 and its higher powers.

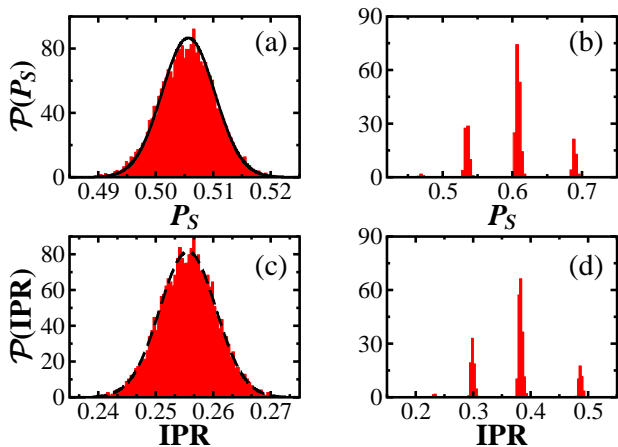


FIG. 4. Distributions of the survival probability [(a), (b)] and inverse participation ratio [(c), (d)] for the GOE [(a), (c)] and the spin [(b), (d)] model at very short times: $t = 0.01$ and $t = 0.5$, respectively. Solid line in (a): theoretical Gaussian distribution with mean from Eq. (13) and variance from Eq. (14), and dashed line in (c): Gaussian with the numerical values for the mean and variance.

1. Survival Probability: GOE model

For the GOE model, the expansion gives

$$\frac{\mathcal{J}_1^2(2\Gamma t)}{\Gamma^2 t^2} = 1 - \Gamma^2 t^2 + \frac{5}{12}\Gamma^4 t^4 - \frac{7}{72}\Gamma^6 t^6 + \frac{7}{480}\Gamma^8 t^8 - \dots$$

As we saw in Eq. (8), Γ^2 is the sum of the square of the off-diagonal elements contained in the row of the Hamiltonian matrix where the initial state lies. For the GOE model, this means the sum of the square of $D - 1$ Gaussian random numbers with $\langle H_{ij} \rangle = 0$ and $\langle H_{ij}^2 \rangle = 1/2$, which gives a χ^2 -distribution with $D - 1$ degrees of freedom. This is approximately a Gaussian distribution with mean $\mu_{\Gamma^2} = (D-1)/2$ and variance $\sigma_{\Gamma^2}^2 = (D-1)/2$.

Using g_n as a notation for the moments of Γ^2 , that is,

$$g_n = \frac{1}{\sqrt{2\pi\sigma_{\Gamma^2}^2}} \int (\Gamma^2)^n \exp\left[-\frac{(\Gamma^2 - \mu_{\Gamma^2})^2}{2\sigma_{\Gamma^2}^2}\right] d\Gamma^2,$$

and keeping terms up to 8th order in time we see that,

$$\langle P_S(t) \rangle \approx 1 - g_1 t^2 + \frac{5}{12} g_2 t^4 - \frac{7}{72} g_3 t^6 + \frac{7}{480} g_4 t^8, \quad (13)$$

and the variance

$$\begin{aligned} \sigma_{P_S(t)}^2 = & \quad (14) \\ & (g_2 - g_1^2)t^4 - \frac{5}{6}(g_3 - g_1 g_2)t^6 \\ & + \left[\frac{25}{144}(g_4 - g_2^2) + \frac{7}{36}(g_4 - g_1 g_3) \right] t^8 \\ & - \left[\frac{7}{240}(g_5 - g_1 g_4) + \frac{35}{432}(g_5 - g_2 g_3) \right] t^{10} \\ & + \left[\frac{49}{5184}(g_6 - g_3^2) + \frac{11}{3600}(g_6 - g_1 g_5) + \frac{7}{576}(g_6 - g_2 g_4) \right] t^{12}. \end{aligned}$$

For a fixed $t = 0.01$ and $D = 12870$, $\langle P_S(0.01) \rangle \sim 0.505$ and $\sigma_{P_S(0.01)}^2 \sim 2.1 \times 10^{-5}$, which are the values used in the Gaussian indicated with a solid line in Fig. 4 (a).

2. Survival Probability: Spin model

For the spin model, the energy E_{ini} [Eq. (4)] of the initial state depends on the disorder strength and on the number n_p of neighboring pairs of up-spins as determined by the Ising interaction, $\sum_k S_k^z S_{k+1}^z$. Focusing only on the Ising interaction, one can see that it leads to $L/2$ energy bands that go from the band of lowest energy with no pairs of up-spins, which has only the two Néel states $|\uparrow\downarrow\uparrow\downarrow\dots\rangle$ and $|\downarrow\uparrow\downarrow\uparrow\dots\rangle$, to the band of highest energy with $n_p = L/2 - 1$ neighboring pairs of up-spins, which has L states [83]. The number of states in a band grows as we approach the middle of the spectrum. The most populated band for chain sizes that are multiple of 4 is centered at energy zero, and for the chains of other even sizes, it is centered at $-1/2$.

The fragmented distribution in Fig. 4 (b) reflects the bands created by the Ising interaction. Each state in a band with n_p pairs of neighboring up-spins couples with $(L - 2n_p)$ other states, and according to Eq. (8), $\Gamma^2 = (L - 2n_p)/4$. For the $L = 16$ case shown in Fig. 4 (b), the states in the most populated band at energy zero has $n_p = 4$ and $\Gamma^2 = 2$, so $P_S(t < \Gamma^{-1}) \sim \exp(-\Gamma^2 t^2)$ gives ~ 0.61 for $t = 0.5$, which is indeed the center of the highest peak in Fig. 4 (b). The two other highest peaks correspond to the Ising band at -1 with $n_p = 3$ and $P_S(0.5) \sim 0.54$ and the band at 1 with $n_p = 5$ and $P_S(0.5) \sim 0.69$.

B. Inverse Participation Ratio and Local Quantities

For small times, the main contribution for $\langle \text{IPR}(t) \rangle$ is the square of the survival probability, $\langle \text{IPR}(t \ll \Gamma^{-1}) \rangle \sim |\langle \Psi(0) | e^{-iHt} | \Psi(0) \rangle|^4$, which explains why the distributions for both quantities are so similar. Compare Fig. 4 (a) with Fig. 4 (c), and Fig. 4 (b) with Fig. 4 (d).

The distributions of the values of the local quantities at short times also reflect the distribution of Γ^2 . They exhibit fragmented structures similar to those in Fig. 4 (b) and Fig. 4 (d).

The main difference between the global and local quantities at short times is that P_S and IPR are not self-averaging, while the local quantities are. This can be understood by comparing, for example, $\mathcal{R}_{P_S}(t)$ and $\mathcal{R}_I(t)$ for the spin model at $t \ll \Gamma^{-1}$. At lowest order in t , we have [16]

$$P_S(t) \sim 1 - \Gamma^2 t^2, \quad (15)$$

so

$$\begin{aligned} \mathcal{R}_{P_S}(t) &\sim \frac{\langle (1 - \Gamma^2 t^2)^2 \rangle - \langle 1 - \Gamma^2 t^2 \rangle^2}{\langle 1 - \Gamma^2 t^2 \rangle^2} \\ &= \sigma_{\Gamma^2}^2 t^4, \end{aligned} \quad (16)$$

which grows with L , since $\sigma_{\Gamma^2}^2 \propto L$. In contrast, the spin autocorrelation function and the other local quantities considered here have an explicit dependence on the system size in the denominator,

$$I(t) \sim 1 - 4 \frac{\Gamma^2 t^2}{L}, \quad (17)$$

so

$$\mathcal{R}_I(t) \sim 16 \frac{\sigma_{\Gamma^2}^2 t^4}{L^2}, \quad (18)$$

which decreases with L .

V. DISTRIBUTIONS AFTER SATURATION

In Fig. 5, we show the distributions of $P_S(t)$ and $\text{IPR}(t)$ after the saturation of the dynamics, for a fixed time $t > t_R$. The distributions for both models are similar, but they differ between the quantities.

As explained in Sec. V C, the distributions for the local quantities $C(t)$ and $I(t)$ are similar to that for $\text{IPR}(t)$. An important discussion in that subsection is how to determine the self-averaging behavior of $|I(t)|$ based on the analysis of the distribution for $I(t)$.

A. Survival Probability

The distribution of $P_S(t)$ for the GOE and the spin model for $t > t_R$ is exponential, as shown in Fig. 5 (a) and Fig. 5 (b). Since the mean and the dispersion of exponential distributions are equal, $\mathcal{R}_{P_S}(t > t_R) \sim 1$ and the survival probability is not self-averaging.

The rate parameter of the distribution of $P_S(t)$ is the reciprocal of the mean of $P_S(t)$, which is given by $1/\sum_{\alpha} |C_{\alpha}^{\text{ini}}|^4$. This can be understood by writing the survival probability as

$$P_S(t) = \sum_{\alpha < \beta} 2|C_{\alpha}^{\text{ini}}|^2 |C_{\beta}^{\text{ini}}|^2 \cos[(E_{\alpha} - E_{\beta})t] + \sum_{\alpha} |C_{\alpha}^{\text{ini}}|^4. \quad (19)$$

On average, the first term on the right hand side of the equation above cancels out, so $\langle P_S(t > t_R) \rangle \sim \sum_{\alpha} |C_{\alpha}^{\text{ini}}|^4$.

The eigenstates of the GOE model are random vectors, so C_{α}^{ini} 's are random numbers from a Gaussian distribution satisfying the constraint $\sum_{\alpha=1}^D |C_{\alpha}^{\text{ini}}|^2 = 1$. Using $\mathcal{P}(C) = \sqrt{D/(2\pi)} e^{-DC^2/2}$ for the components, we have $\langle C \rangle = 0$, $\langle C^2 \rangle = 1/D$, and $\langle C^4 \rangle = 3/D^2$, so $\sum_{\alpha} |C_{\alpha}^{\text{ini}}|^4 = \sum_{\alpha} (3/D^2) = 3/D$.

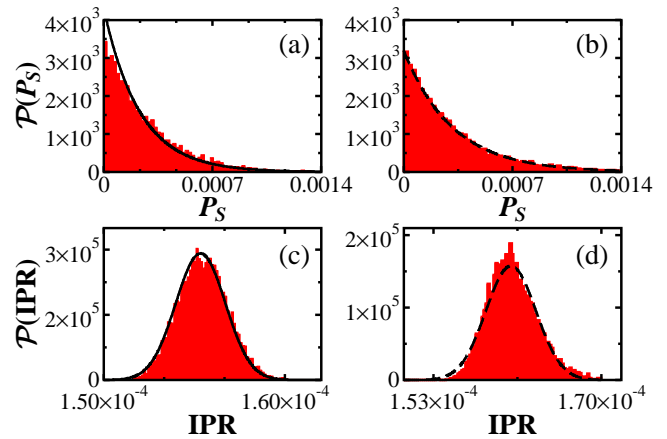


FIG. 5. Distributions of the survival probability [(a), (b)] and inverse participation ratio [(c), (d)] for the GOE model [(a), (c)] at $t = 10^3$ and for the spin model [(b), (d)] at $t = 5 \times 10^4$. Solid lines in (a): exponential distribution with rate parameter $D/3$; in (c): Gaussian distribution with mean and variance from Eq. (22) and Eq. (23). Dashed lines in (b): exponential distribution with rate parameter $1/\langle \sum_{\alpha} |C_{\alpha}^{\text{ini}}|^4 \rangle$; and in (d): Gaussian curve with the numerical values for $\langle \text{IPR}(t) \rangle$ and $\sigma_{\text{IPR}}(t)$ at $t = 5 \times 10^4$.

For the chaotic spin model, the eigenstates away from the edges of the spectrum are also approximately random vectors, so $\sum_{\alpha} |C_{\alpha}^{\text{ini}}|^4$ is close to $3/D$, although slightly larger. This discrepancy becomes particularly evident if one tries to fit the numerical distribution in Fig. 5 (b) with a single parameter. The fact that we get a value slightly larger than $3/D$ suggests some remaining level of correlations between the components of the initial state.

A simple justification for the exponential shape of the distribution for $P_S(t)$ can be given by substituting

$$\left| \sum_{\alpha} |C_{\alpha}^{\text{ini}}|^2 e^{-iE_{\alpha}t} \right|^2$$

with

$$\frac{1}{D^2} \left\{ \left[\sum_{\alpha} \cos(E_{\alpha}t) \right]^2 + \left[\sum_{\alpha} \sin(E_{\alpha}t) \right]^2 \right\}.$$

The sum of the cosines and the sum of the sines are Gaussian random variables. This was shown in [29] for full random matrices and we verified numerically that it holds also when E_{α} are random numbers from a Gaussian distribution and $t > t_R$. The distribution of the sum of the square of two Gaussian random numbers is exponential, which explains the shape seen in Fig. 5 (a) and Fig. 5 (b). Notice, however, that this simplification gives $1/D$ as the mean value for $P_S(t)$, which differs from the correct value by a factor of 3.

The proper derivation of the exponential distribution for $P_S(t)$ involves the convolution of the distribution for the components of the initial state with the distribution

for $e^{-iE_\alpha t}$, as done in [30] for random matrices. The result for $t > t_R$ is

$$\mathcal{P}(P_S) = \frac{1}{\sum_\alpha |C_\alpha^{\text{ini}}|^4} \exp \left[-\frac{P_S(t)}{\sum_\alpha |C_\alpha^{\text{ini}}|^4} \right]. \quad (20)$$

The agreement between this theoretical curve and the numerical distribution of $P_S(t)$ for the GOE and the spin model is excellent, as seen in Fig. 5 (a) and Fig. 5 (b).

B. Inverse Participation Ratio

The distribution of the inverse participation ratio for the GOE and the spin model at a fixed time $t > t_R$ is Gaussian, as evident in Fig. 5 (c) and Fig. 5 (d). Similarly to the discussion for the survival probability, this shape may be justified by looking at the distribution of the sum of the square of normal random variables. In the case of the inverse participation ratio, this is a large sum, since

$$\text{IPR}(t) = \sum_n \left| \sum_\alpha C_\alpha^n C_\alpha^{\text{ini}} e^{-E_\alpha t} \right|^4, \quad (21)$$

so the sum leads to a Gaussian distribution. Following the steps described in [30], it should be possible to formally derive the Gaussian distribution by doing the convolutions between the distributions for the components C_α^n and C_α^{ini} and for $e^{-E_\alpha t}$ and taking into account the sum over all basis vectors $|n\rangle$.

The mean of the distribution of $\text{IPR}(t)$ is obtained by using that the only terms in

$$\text{IPR}(t) = \sum_n \sum_{\alpha, \beta, \gamma, \delta} C_\alpha^n C_\alpha^{\text{ini}} C_\beta^m C_\beta^{\text{ini}} C_\gamma^n C_\gamma^{\text{ini}} C_\delta^m C_\delta^{\text{ini}} e^{-(E_\alpha - E_\beta + E_\gamma - E_\delta)t}$$

that do not average out at long times are those where $\alpha = \beta, \gamma = \delta$, with $\alpha \neq \delta; \alpha = \delta, \beta = \gamma$, with $\alpha \neq \beta$; and $\alpha = \beta = \gamma = \delta$, which gives

$$2 \sum_n \left(\sum_\alpha |C_\alpha^n|^2 |C_\alpha^{\text{ini}}|^2 \right)^2 - \sum_\alpha |C_\alpha^{\text{ini}}|^4 \left(\sum_n |C_\alpha^n|^4 \right).$$

Since $|C_\alpha^n|^2 \sim 1/D$, we have

$$\frac{2}{D} - \frac{9}{D^2}. \quad (22)$$

To compute the variance of the distribution, we need the dominant terms of

$$\begin{aligned} \text{IPR}^2(t) = & \sum_n \sum_{\alpha, \beta, \gamma, \delta} \sum_{n'} \sum_{\alpha', \beta', \gamma', \delta'} \\ & \times C_\alpha^n C_\alpha^{\text{ini}} C_\beta^m C_\beta^{\text{ini}} C_\gamma^n C_\gamma^{\text{ini}} C_\delta^m C_\delta^{\text{ini}} e^{-(E_\alpha - E_\beta + E_\gamma - E_\delta)t} \\ & \times C_{\alpha'}^{n'} C_{\alpha'}^{\text{ini}} C_{\beta'}^{m'} C_{\beta'}^{\text{ini}} C_{\gamma'}^{n'} C_{\gamma'}^{\text{ini}} C_{\delta'}^{m'} C_{\delta'}^{\text{ini}} e^{-(E_{\alpha'} - E_{\beta'} + E_{\gamma'} - E_{\delta'})t}. \end{aligned}$$

There are four terms similar to the one with $\alpha = \beta, \alpha' = \beta', \gamma = \delta, \gamma' = \delta'$, which gives $4 \sum_n (\sum_\alpha |C_\alpha^n|^2 |C_\alpha^{\text{ini}}|^2)^2 - 4 \sum_\alpha |C_\alpha^{\text{ini}}|^4 (\sum_n |C_\alpha^n|^4)$ and they cancel the dominant terms of $\langle \text{IPR}(t > t_R) \rangle^2$, so they do not contribute to the variance. But there are also four terms similar to the one with $\alpha = \delta, \alpha' = \delta', \beta = \gamma, \beta' = \gamma'$, which for $n = n'$ gives

$$4 \sum_n \sum_{\alpha, \beta, \gamma, \delta} |C_\alpha^n|^2 |C_\alpha^{\text{ini}}|^2 |C_\beta^n|^2 |C_\beta^{\text{ini}}|^2 |C_\gamma^n|^2 |C_\gamma^{\text{ini}}|^2 |C_\delta^n|^2 |C_\delta^{\text{ini}}|^2,$$

so the variance of the distribution of $\text{IPR}(t)$ for a fixed $t > t_R$ is

$$\sigma_{\text{IPR}}^2 \sim \frac{4}{D^3}. \quad (23)$$

The Gaussian distribution with the mean from Eq. (22) and the variance from Eq. (23) matches very well the histogram for the GOE model in Fig. 5 (c). Furthermore, our numerical analysis of the distributions obtained for random matrices of different sizes shows that the skewness $\rightarrow 0$ and the kurtosis $\rightarrow 3$ as the dimension of the matrices increases, just as we would expect for a symmetric Gaussian distribution.

For the spin model, the dashed line in Fig. 5 (d) is a Gaussian curve with the numerical values obtained for $\langle \text{IPR}(t) \rangle$ and $\sigma_{\text{IPR}}^2(t)$ for a fixed $t > t_R$. The mean and variance for this curve are slightly larger than the values in Eq. (22) and Eq. (23) suggesting some level of correlation between the components of the eigenstates of the realistic model. We might expect the results to approach those for the GOE model as L increases, although our numerical analysis of the distributions for $L = 10, 12, 14, 16, 18$ indicates that the skewness $\rightarrow 1$ and the kurtosis $\rightarrow 4$ as the system size increases. These values indicate a non-symmetric distribution with heavier tails than a Gaussian distribution.

The results for the mean and variance of $\text{IPR}(t)$ in Eq. (22) and Eq. (23) make it clear that $\mathcal{R}_{\text{IPR}}(t)$ decreases as $1/D$ and therefore, the inverse participation ratio becomes self-averaging at long times. The dependence of $\mathcal{R}_{\text{IPR}}(t > t_R)$ on the dimension of the Hamiltonian matrix instead of the system size L is characteristic of interacting many-body quantum systems. This is related to the fact that the spread of the initial state takes place in the many-body Hilbert space instead of the real space.

C. Local Quantities

The distributions for the spin autocorrelation function and the connected spin-spin correlation function at long times are Gaussian (not shown). We also verify that the distribution for $|I(t > t_R)|$ is a folded Gaussian, which further supports that the distribution for $I(t > t_R)$ is indeed Gaussian. However, $C(t)$ is strongly self-averaging, with $\mathcal{R}_C(t > t_R)$ decreasing exponentially as L increases

(see Ref. [16]), while according to Fig. 3 (c), $I(t)$ is non-self-averaging at long times. This is what we observe by studying system sizes with $L \leq 18$, although one cannot rule out the possibility that this behavior might change for much larger L 's. Based on the results at hand, the fact that both quantities exhibit a Gaussian distribution makes us conclude that there is no direct connection between self-averaging for $t > t_R$ and the shape of the distributions.

Among the scaling analysis in Fig. 3 (f), the least conclusive one is that for $|I(t)|$. It suggests lack of self-averaging at long times, but larger system sizes are needed for a more definite answer. Yet, we can circumvent this limitation and use the numerical results for $I(t)$ to infer the self-averaging behavior of $|I(t)|$, as we explain next.

Both the standard deviation and the mean of $I(t)$ for $t > t_R$ decrease as the system size increases. The exponents s and m in $\sigma_I(t > t_R) \propto L^{-s}$ and $\langle I(t > t_R) \rangle \propto L^{-m}$ can be obtained numerically. We find that $m > s$. With this information, we can compute the mean and the variance of the folded Gaussian distribution for $|I(t)|$ using

$$\begin{aligned} \langle |I| \rangle &= \sqrt{\frac{2}{\pi}} \sigma_I \exp\left(-\frac{\langle I \rangle^2}{2\sigma_I^2}\right) + \langle I \rangle \operatorname{erf}\left(\frac{\langle I \rangle}{\sigma_I}\right) \\ \sigma_{|I|}^2 &= \langle I \rangle^2 + \sigma_I^2 - \langle |I| \rangle^2. \end{aligned}$$

For large L , we find that

$$\langle |I| \rangle \rightarrow L^{-s} \sqrt{\frac{2}{\pi}}, \quad (24)$$

$$\sigma_{|I|}^2 \rightarrow L^{-2s} \left(1 - \frac{2}{\pi}\right), \quad (25)$$

which implies that the relative variance goes asymptotically to a constant,

$$\mathcal{R}_{|I|}(t > t_R) \rightarrow \frac{\pi - 2}{2} \sim 0.57. \quad (26)$$

This value is indeed very close to what we have in Fig. 3 (f), but the semi-analytical strategy described above provides a much stronger evidence that $|I(t)|$ is non-self-averaging at long times than what we can conclude from the numerical results in Fig. 3 (f).

VI. DISTRIBUTIONS AT INTERMEDIATE TIMES

As time grows from zero, the distributions for the various quantities studied here gradually change their shapes from those observed at short times to those at long times. Illustrations of the distributions for $P_S(t)$ and $\text{IPR}(t)$ for the spin model at intermediate times are shown in Fig. 6.

A. Survival Probability

As time increases, the Gaussian distribution that $P_S(t)$ shows for the GOE model at short times becomes gradually more skewed until an exponential distribution emerges. For the spin model, the bands found in the distribution at short times [Fig. 6 (a)] broaden and simultaneously become more skewed [Fig. 6 (b)] until the distribution becomes exponential as well.

Notice that for both models, the exponential distribution is seen before t_R . It starts taking shape already in the interval of the power-law decay [Fig. 6 (c)] and it becomes clearly exponential when the spectral correlations get manifested in the dynamics and the correlation hole develops [Figs. 6 (d) and (e)].

For $t \geq t_{\text{Th}}$, the rate parameter of the exponential distribution is given by $1/\langle P_S(t) \rangle$, as shown with a dashed line in Fig. 6 (d) and Fig. 6 (e). It is only for $t > t_R$ that $1/\langle P_S(t) \rangle \sim 1/\sum_{\alpha} |C_{\alpha}^{\text{ini}}|^4$ and we recover the curve from Fig. 5 (b). The fact that we have an exponential distribution for $P_S(t)$, with mean equal to the dispersion during the entire duration of the correlation hole, implies that both $\langle P_S(t) \rangle$ and $\sigma_{P_S}(t)$ decrease below their saturation values and that $\mathcal{R}_{P_S}(t) \sim 1$ for any time $t \geq t_{\text{Th}}$.

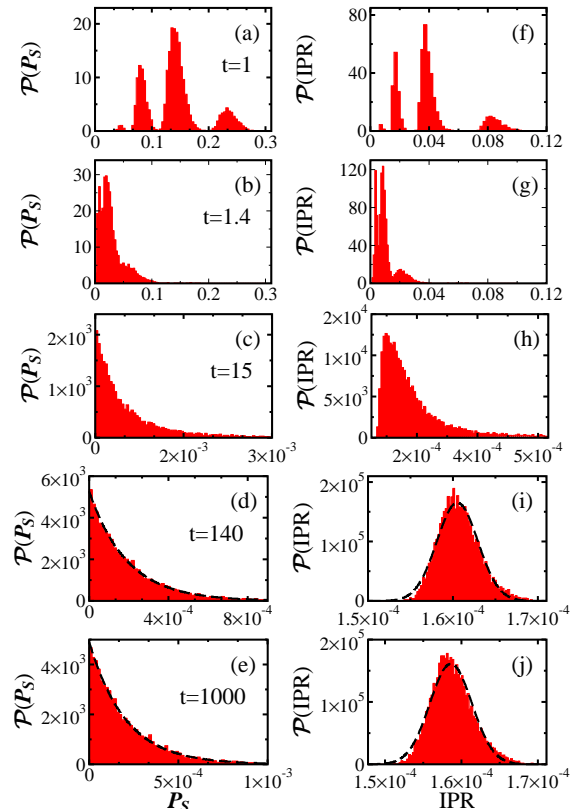


FIG. 6. Distributions of the survival probability (left) and inverse participation ratio (right) for the spin at times indicated in the panels. Dashed lines in (d) and (e): exponential distribution with rate parameter given by $1/\langle P_S(t) \rangle$; in (i) and (j): Gaussian distribution with the mean and variance obtained numerically.

B. Inverse Participation Ratio and Local Quantities

The distribution of $\text{IPR}(t)$ for the GOE model is throughout Gaussian, although some level of skewness and kurtosis larger than 3 are seen for times where $\langle \text{IPR}(t) \rangle$ oscillates, which corresponds to the power-law region of the survival probability. The width of the distribution depends on the dimension of the GOE matrix. At short times, the variance is related with the distribution of Γ^2 , so it increases as the matrix grows, while at long times, the variance is related with the distributions of the components C_α^n , so it decreases as D grows. The fact that the distribution is Gaussian at short and long times, but self-averaging holds at long times only, reiterates our claim that there is not a one to one correspondence between the shape of the distribution and the presence of self-averaging.

The distribution for $\text{IPR}(t)$ for the spin model is hybrid. It starts similar to the distribution for survival probability of the spin model [Fig. 6 (f) and Fig. 6 (g)], but later it acquires a shape equivalent to the distribution of $\text{IPR}(t)$ for the GOE model [Fig. 6 (i) and Fig. 6 (j)].

The distributions for the connected spin-spin correlation function and the spin autocorrelation function in the spin model progress in time in a way similar to the distribution for the inverse participation ratio, from a fragmented structure at short times to a Gaussian shape at long times.

VII. CONCLUSIONS

We investigated the distributions over disorder realizations of different quantities in a realistic chaotic spin model at different time scales, from very short times up to equilibration, and compared the results with the self-averaging properties of these quantities. The distributions for the global quantities – the survival probability and the inverse participation ratio – were contrasted also with those for the GOE model. They are comparable at long times, but not at short times.

At long times, the distribution of the survival probability for both models is exponential, which accounts for the lack of self-averaging of this quantity. The exponential shape emerges when the dynamics detect spectral correlations typical of chaotic systems.

At long times, the distribution of the inverse participation ratio and also of the local quantities – the spin-spin correlation function and the spin autocorrelation function – are Gaussian. The fact that the first two are self-averaging, while the spin autocorrelation function is not demonstrates that there is not a direct relationship between the presence of self-averaging and the shape of the distribution.

We also studied the absolute value and the square of the spin autocorrelation function, $|I(t)|$ and $I^2(t)$. The evolution of their mean values shows features similar to those observed for $\langle I(t) \rangle$, but their self-averaging behaviors differ. Based on the system sizes available, we conclude that at long times the spin autocorrelation function is non-self-averaging, while $I^2(t)$ is. The numerical scaling analysis of the relative variance of $|I(t)|$ is less conclusive.

A main result of this work is to show that knowledge of the distribution of one quantity may be used to uncover the self-averaging behavior of another related quantity. This is what we did using $I(t)$ and $|I(t)|$ as an example. Starting with the Gaussian distribution and non-self-averaging behavior of $I(t)$ at long times, we showed that the relative variance of $|I(t)|$ for times $t > t_R$ goes asymptotically to a constant as L increases. This strategy circumvents the limitation of the numerical scaling analysis to small system sizes and allows us to deduce that $|I(t)|$ is non-self-averaging at long times.

ACKNOWLEDGMENTS

We are grateful to Mauro Schiulaz for various discussions during the beginning of this project. E.J.T.-H. and I.V.-F. acknowledge funding from VIEP-BUAP (Grant Nos. MEBJ-EXC19-G, LUAGEXC19-G), Mexico. They are also grateful to LNS-BUAP for allowing use of their supercomputing facility. L.F.S. is supported by the NSF Grant No. DMR-1936006.

-
- [1] Hannes Bernien, Sylvain Schwartz, Alexander Keesling, Harry Levine, Ahmed Omran, Hannes Pichler, Soonwon Choi, Alexander S. Zibrov, Manuel Endres, Markus Greiner, Vladan Vuletić, and Mikhail D. Lukin, “Probing many-body dynamics on a 51-atom quantum simulator,” *Nature* **551**, 579–584 (2017).
- [2] W. L. Tan and et al, “Observation of domain wall confinement and dynamics in a quantum simulator,” *ArXiv:1912.11117*.
- [3] John M. Martinis, Michel H. Devoret, and John Clarke, “Quantum josephson junction circuits and the dawn of artificial atoms,” *Nat. Phys.* **16**, 234–237 (2020).
- [4] Mohamad Niknam, Lea F. Santos, and David G. Cory, “Sensitivity of quantum information to environment perturbations measured with a nonlocal out-of-time-order correlation function,” *Phys. Rev. Research* **2**, 013200 (2020).
- [5] C. M. Sánchez, A. K. Chattah, K. X. Wei, L. Buljubasich, P. Cappellaro, and H. M. Pastawski, “Perturbation independent decay of the loschmidt echo in a many-body system,” *Phys. Rev. Lett.* **124**, 030601 (2020).
- [6] M. Rigol, V. Dunjko, and M. Olshanii, “Thermaliza-

- tion and its mechanism for generic isolated quantum systems,” *Nature* **452**, 854 EP – (2008).
- [7] L. F. Santos and M. Rigol, “Onset of quantum chaos in one-dimensional bosonic and fermionic systems and its relation to thermalization,” *Phys. Rev. E* **81**, 036206 (2010).
- [8] E. J. Torres-Herrera and Lea F. Santos, “Effects of the interplay between initial state and Hamiltonian on the thermalization of isolated quantum many-body systems,” *Phys. Rev. E* **88**, 042121 (2013).
- [9] F. Borgonovi, F. M. Izrailev, L. F. Santos, and V. G. Zelevinsky, “Quantum chaos and thermalization in isolated systems of interacting particles,” *Phys. Rep.* **626**, 1 (2016).
- [10] L. D’Alessio, Y. Kafri, A. Polkovnikov, and M. Rigol, “From quantum chaos and eigenstate thermalization to statistical mechanics and thermodynamics,” *Adv. Phys.* **65**, 239–362 (2016).
- [11] I. Bloch, J. Dalibard, and S. Nascimbène, “Quantum simulations with ultracold quantum gases,” *Nat. Phys.* **8**, 267–276 (2012).
- [12] Lea F. Santos and Aditi Mitra, “Domain wall dynamics in integrable and chaotic spin-1/2 chains,” *Phys. Rev. E* **84**, 016206 (2011).
- [13] Dominique Gobert, Corinna Kollath, Ulrich Schollwöck, and Gunter Schütz, “Real-time dynamics in spin- $\frac{1}{2}$ chains with adaptive time-dependent density matrix renormalization group,” *Phys. Rev. E* **71**, 036102 (2005).
- [14] Mauro Schiulaz, E. Jonathan Torres-Herrera, and Lea F. Santos, “Thouless and relaxation time scales in many-body quantum systems,” *Phys. Rev. B* **99**, 174313 (2019).
- [15] Anatoly Dymarsky, “Mechanism of macroscopic equilibration of isolated quantum systems,” *Phys. Rev. B* **99**, 224302 (2019).
- [16] Mauro Schiulaz, E. Jonathan Torres-Herrera, Francisco Pérez-Bernal, and Lea F. Santos, “Self-averaging in many-body quantum systems out of equilibrium: Chaotic systems,” *Phys. Rev. B* **101**, 174312 (2020).
- [17] E. Jonathan Torres-Herrera, Mauro Schiulaz, Francisco Pérez-Bernal, and Lea F. Santos, “Self-averaging behavior at the metal-insulator transition of many-body quantum systems out of equilibrium,” *ArXiv:1910.11332*.
- [18] Jonas Richter, Dennis Schubert, and Robin Steinigeweg, “Decay of spin-spin correlations in disordered quantum and classical spin chains,” *Phys. Rev. Research* **2**, 013130 (2020).
- [19] M. Serbyn, Z. Papić, and D. A. Abanin, “Thouless energy and multifractality across the many-body localization transition,” *Phys. Rev. B* **96**, 104201 (2017).
- [20] S. Wiseman and E. Domany, “Lack of self-averaging in critical disordered systems,” *Phys. Rev. E* **52**, 3469 (1995).
- [21] A. Aharony and A. B. Harris, “Absence of self-averaging and universal fluctuations in random systems near critical points,” *Phys. Rev. Lett.* **77**, 3700 (1996).
- [22] S. Wiseman and E. Domany, “Finite-size scaling and lack of self-averaging in critical disordered systems,” *Phys. Rev. Lett.* **81**, 22 (1998).
- [23] T. Castellani and A. Cavagna, “Spin-glass theory for pedestrians,” *J. Stat. Mech. Th. Exp.* **2005**, P05012 (2005).
- [24] A. Malakis and N. G. Fytas, “Lack of self-averaging of the specific heat in the three-dimensional random-field Ising model,” *Phys. Rev. E* **73**, 016109 (2006).
- [25] S. Roy and S. M. Bhattacharjee, “Is small-world network disordered?” *Phys. Lett. A* **352**, 13 (2006).
- [26] C. Monthus, “Random Walks and Polymers in the Presence of Quenched Disorder,” *Lett. Math. Phys.* **78**, 207 (2006).
- [27] A. Efrat and M. Schwartz, “Lack of self-averaging in random systems - Liability or asset?” *Phys. A Stat. Mech. Appl.* **414**, 137 (2014).
- [28] R. E. Prange, “The spectral form factor is not self-averaging,” *Phys. Rev. Lett.* **78**, 2280 (1997).
- [29] Hervé Kunz, “The probability distribution of the spectral form factor in random matrix theory,” *J.Phys. A* **32**, 2171–2182 (1999).
- [30] H. Kunz, “Quantum dynamics and random matrix theory,” *Int. J. Mod. Phys. B* **16**, 2003–2008 (2002), <https://doi.org/10.1142/S0217979202011731>.
- [31] M. L. Mehta, *Random Matrices* (Academic Press, Boston, USA, 1991).
- [32] Fritz Haake, *Quantum Signatures of Chaos* (Springer-Verlag, Berlin, 1991).
- [33] T. Guhr, A. Mueller-Gröeling, and H. A. Weidenmüller, “Random matrix theories in quantum physics: Common concepts,” *Phys. Rep.* **299**, 189 (1998).
- [34] V. Zelevinsky, B. A. Brown, N. Frazier, and M. Horoi, “The nuclear shell model as a testing ground for many-body quantum chaos,” *Phys. Rep.* **276**, 85–176 (1996).
- [35] Nathan Argaman, Yoseph Imry, and Uzy Smilansky, “Semiclassical analysis of spectral correlations in mesoscopic systems,” *Phys. Rev. B* **47**, 4440–4457 (1993).
- [36] In Refs. [14, 16], $H = (M + M^T)/\sqrt{2}$ was used, which gives $\langle H_{ii}^2 \rangle = 2$ and $\langle H_{i \neq j}^2 \rangle = 1$. In Ref. [38], $H = M + M^T$, so $\langle H_{ii}^2 \rangle = 4$ and $\langle H_{i \neq j}^2 \rangle = 2$.
- [37] E. P. Wigner, “On the distribution of the roots of certain symmetric matrices,” *Ann. Math.* **67**, 325 (1958).
- [38] E. J. Torres-Herrera, Antonio M. García-García, and Lea F. Santos, “Generic dynamical features of quenched interacting quantum systems: Survival probability, density imbalance, and out-of-time-ordered correlator,” *Phys. Rev. B* **97**, 060303 (2018).
- [39] M. Schreiber, S. S. Hodgman, Pr. Bordia, H. P. Lüschen, M. H. Fischer, R. Vosk, E. Altman, U. Schneider, and I. Bloch, “Observation of many-body localization of interacting fermions in a quasirandom optical lattice,” *Science* **349**, 842–845 (2015).
- [40] L. F. Santos, G. Rigolin, and C. O. Escobar, “Entanglement versus chaos in disordered spin systems,” *Phys. Rev. A* **69**, 042304 (2004).
- [41] F. Dukesz, M. Zilbergerts, and L. F. Santos, “Interplay between interaction and (un)correlated disorder in one-dimensional many-particle systems: delocalization and global entanglement,” *New J. Phys.* **11**, 043026 (2009).
- [42] Arijeet Pal and David A. Huse, “Many-body localization phase transition,” *Phys. Rev. B* **82**, 174411 (2010).
- [43] R. Nandkishore and D.A. Huse, “Many-body localization and thermalization in quantum statistical mechanics,” *Annu. Rev. Condens. Matter Phys.* **6**, 15 (2015).
- [44] E. J. Torres-Herrera and Lea F. Santos, “Extended non-ergodic states in disordered many-body quantum systems,” *Ann. Phys. (Berlin)* **529**, 1600284 (2017).
- [45] D. Luitz and Y. Bar Lev, “The ergodic side of the many-body localization transition,” *Ann. Phys.(Berlin)* **529**, 1600350 (2017).
- [46] Y. Avishai, J. Richert, and R. Berkovits, “Level statistics

- in a Heisenberg chain with random magnetic field,” *Phys. Rev. B* **66**, 052416 (2002).
- [47] L. F. Santos, “Integrability of a disordered Heisenberg spin-1/2 chain,” *J. Phys. A* **37**, 4723–4729 (2004).
- [48] E. J. Torres-Herrera, D. Kollmar, and L. F. Santos, “Relaxation and thermalization of isolated many-body quantum systems,” *Phys. Scr. T* **165**, 014018 (2015).
- [49] K. Singh, C. J. Fujiwara, Z. A. Geiger, E. Q. Simmons, M. Lipatov, A. Cao, P. Dotti, S. V. Rajagopal, R. Senaratne, T. Shimasaki, M. Heyl, A. Eckardt, and D. M. Weld, “Quantifying and controlling prethermal nonergodicity in interacting floquet matter,” *Phys. Rev. X* **9**, 041021 (2019).
- [50] K. Bhattacharyya, “Quantum decay and the Mandelstam-Tamm-energy inequality,” *J. Phys. A* **16**, 2993 (1983).
- [51] J. Ufink, “The rate of evolution of a quantum state,” *Am. J. Phys.* **61**, 935–936 (1993).
- [52] Ph. Jacquod, P.G. Silvestrov, and C.W.J. Beenakker, “Golden rule decay versus lyapunov decay of the quantum loschmidt echo,” *Phys. Rev. E* **64**, 055203 (2001).
- [53] Nicholas R. Cerruti and Steven Tomsovic, “Sensitivity of wave field evolution and manifold stability in chaotic systems,” *Phys. Rev. Lett.* **88**, 054103 (2002).
- [54] L. A. Khalfin, “Contribution to the decay theory of a quasi-stationary state,” *Sov. Phys. JETP* **6**, 1053 (1958).
- [55] J. G. Muga, A. Ruschhaupt, and A. del Campo, *Time in Quantum Mechanics, vol. 2* (Springer, London, 2009).
- [56] A. del Campo, “Exact quantum decay of an interacting many-particle system: the Calogero–Sutherland model,” *N. J. Phys.* **18**, 015014 (2016).
- [57] Marco Távora, E. J. Torres-Herrera, and Lea F. Santos, “Inevitable power-law behavior of isolated many-body quantum systems and how it anticipates thermalization,” *Phys. Rev. A* **94**, 041603 (2016).
- [58] Marco Távora, E. J. Torres-Herrera, and Lea F. Santos, “Power-law decay exponents: A dynamical criterion for predicting thermalization,” *Phys. Rev. A* **95**, 013604 (2017).
- [59] E. J. Torres-Herrera and Lea F. Santos, “Quench dynamics of isolated many-body quantum systems,” *Phys. Rev. A* **89**, 043620 (2014).
- [60] E. J. Torres-Herrera, M Vyas, and Lea F. Santos, “General features of the relaxation dynamics of interacting quantum systems,” *New J. Phys.* **16**, 063010 (2014).
- [61] E. J. Torres-Herrera and Lea F. Santos, “Local quenches with global effects in interacting quantum systems,” *Phys. Rev. E* **89**, 062110 (2014).
- [62] Paolo P Mazza, Jean-Marie Stéphan, Elena Canovi, Vincenzo Alba, Michael Brockmann, and Masudul Haque, “Overlap distributions for quantum quenches in the anisotropic Heisenberg chain,” *J. Stat. Mech.* **2016**, 013104 (2016).
- [63] Sergio Lerma-Hernández, Jorge Chávez-Carlos, Miguel A Bastarrachea-Magnani, Lea F Santos, and Jorge G Hirsch, “Analytical description of the survival probability of coherent states in regular regimes,” *J. Phys. A* **51**, 475302 (2018).
- [64] A. Volya and V. Zelevinsky, “Time-dependent relaxation of observables in complex quantum systems,” *ArXiv:1905.11918*.
- [65] M. Heyl, A. Polkovnikov, and S. Kehrein, “Dynamical quantum phase transitions in the transverse-field Ising model,” *Phys. Rev. Lett.* **110**, 135704 (2013).
- [66] Lea F. Santos, Marco Távora, and Francisco Pérez-Bernal, “Excited-state quantum phase transitions in many-body systems with infinite-range interaction: Localization, dynamics, and bifurcation,” *Phys. Rev. A* **94**, 012113 (2016).
- [67] Eric J. Heller, “Bound-state eigenfunctions of classically chaotic hamiltonian systems: Scars of periodic orbits,” *Physical Review Letters* **53**, 1515–1518 (1984).
- [68] David Villasenor, Saúl Pilatowsky-Cameo, Miguel A. Bastarrachea-Magnani, Sergio Lerma-Hernández, Lea F. Santos, and Jorge G. Hirsch, “Quantum vs classical dynamics in a spin-boson system: manifestations of spectral correlations and scarring,” *ArXiv:2002.02465*.
- [69] R. Ketzmerick, G. Petschel, and T. Geisel, “Slow decay of temporal correlations in quantum systems with Cantor spectra,” *Phys. Rev. Lett.* **69**, 695–698 (1992).
- [70] Alexander D. Mirlin, “Statistics of energy levels and eigenfunctions in disordered systems,” *Phys. Rep.* **326**, 259 – 382 (2000).
- [71] E. J. Torres-Herrera and Lea F. Santos, “Dynamics at the many-body localization transition,” *Phys. Rev. B* **92**, 014208 (2015).
- [72] Soumya Bera, Giuseppe De Tomasi, Ivan M. Khaymovich, and Antonello Scardicchio, “Return probability for the Anderson model on the random regular graph,” *Phys. Rev. B* **98**, 134205 (2018).
- [73] Luc Leviandier, Maurice Lombardi, Rémi Jost, and Jean Paul Pique, “Fourier transform: A tool to measure statistical level properties in very complex spectra,” *Phys. Rev. Lett.* **56**, 2449–2452 (1986).
- [74] Joshua Wilkie and Paul Brumer, “Time-dependent manifestations of quantum chaos,” *Phys. Rev. Lett.* **67**, 1185–1188 (1991).
- [75] Y. Alhassid and R. D. Levine, “Spectral autocorrelation function in the statistical theory of energy levels,” *Phys. Rev. A* **46**, 4650–4653 (1992).
- [76] E. J. Torres-Herrera and Lea F. Santos, “Dynamical manifestations of quantum chaos: correlation hole and bulge,” *Philos. Trans. Royal Soc. A* **375**, 20160434 (2017).
- [77] S. Lerma-Hernández, D. Villaseñor, M. A. Bastarrachea-Magnani, E. J. Torres-Herrera, L. F. Santos, and J. G. Hirsch, “Dynamical signatures of quantum chaos and relaxation time scales in a spin-boson system,” *Phys. Rev. E* **100**, 012218 (2019).
- [78] Javier de la Cruz, Sergio Lerma-Hernandez, and Jorge G. Hirsch, “Quantum chaos in a system with high degree of symmetries,” *ArXiv:2005.06589*.
- [79] Fausto Borgonovi, Felix M. Izrailev, and Lea F. Santos, “Exponentially fast dynamics of chaotic many-body systems,” *Phys. Rev. E* **99**, 010101 (2019).
- [80] Fausto Borgonovi, Felix M. Izrailev, and Lea F. Santos, “Timescales in the quench dynamics of many-body quantum systems: Participation ratio versus out-of-time ordered correlator,” *Phys. Rev. E* **99**, 052143 (2019).
- [81] P. Richerme, Z.-X. Gong, A. Lee, Cr. Senko, J. Smith, M. Foss-Feig, S. Michalakis, A. V. Gorshkov, and C. Monroe, “Non-local propagation of correlations in quantum systems with long-range interactions,” *Nature* **511**, 198–201 (2014).
- [82] E. Jonathan Torres-Herrera and Lea F. Santos, “Signatures of chaos and thermalization in the dynamics of many-body quantum systems,” *Eur. Phys. J. Spec. Top.* **227**, 1897–1910 (2019).

- [83] Kira Joel, Davida Kollmar, and Lea F. Santos, “An introduction to the spectrum, symmetries, and dynamics of spin-1/2 Heisenberg chains,” *American Journal of Physics* **81**, 450–457 (2013).